Accepted for Publication in AJ
Preprint typeset using LaTeX style emulateapj v. 10/09/06

arXiv:0908.0741v1 [astro-ph.CO] 5 Aug 2009

KINEMATIC AND PHOTOMETRIC EVIDENCE FOR A BAR IN NGC 2683

Rachel Kuzio de Naray[1]
Center for Cosmology, Department of Physics and Astronomy, University of California, Irvine, CA 92697-4575
and
Matthew J. Zagursky and Stacy S. McGaugh
Department of Astronomy, University of Maryland, College Park, MD 20742-2421

Accepted for Publication in AJ

ABSTRACT

We present optical long-slit and SparsePak Integral Field Unit emission line spectroscopy along with optical broadband and near IR images of the edge-on spiral galaxy NGC 2683. We find a multi-valued, figure-of-eight velocity structure in the inner 45″ of the long-slit spectrum and twisted isovelocity contours in the velocity field. We also find, regardless of wavelength, that the galaxy isophotes are boxy. We argue that taken together, these kinematic and photometric features are evidence for the presence of a bar in NGC 2683. We use our data to constrain the orientation and strength of the bar.

Subject headings: galaxies: bulges — galaxies: kinematics and dynamics — galaxies: spiral — galaxies: structure

1. INTRODUCTION

A large fraction of edge-on spiral galaxies have been observed to have boxy or peanut-shaped (hereafter B/PS) bulges. As the observations have improved and the samples have grown, the percentage of galaxies with these bulge shapes has increased from less than 20% (Jarvis 1986; Shaw 1987; de Souza & dos Anjos 1987) to up to 45% (Lütticke, Dettmar, & Pohlen 2000a). Because the observed frequency of B/PS bulges is so high, significant effort has been invested in determining the formation mechanism responsible for these bulge shapes.

Binney & Petrou (1985) and Rowley (1988) demonstrated that the accretion of satellite galaxies could result in a galaxy bulge looking boxy or peanut-shaped. The currently favored formation mechanism, however, is the buckling and subsequent vertical thickening of a bar (e.g. Combes & Sanders 1981; Combes et al 1990; Raha et al. 1991).

This is a plausible explanation, as bars are known to be common features in disk galaxies. Whyte et al. (2002) found that 79% of disk galaxies are barred in the near-infrared and 74% are barred in the optical (see also Eskridge et al. 2000; Marinova & Jogee 2007). Barred galaxies are also known to occur in a variety of environments. Using a sample of 930 galaxies, van den Bergh (2002) showed that the presence of a bar does not depend on whether the galaxy is in the field or is a member of a group or a cluster. Similarly, Verley et al. (2007) studied the bar frequency in isolated galaxies and found roughly equal numbers of barred and unbarred systems.

To confirm the bar buckling hypothesis, bars must be detected in edge-on galaxies with B/PS bulges. While bars can be easily seen in face-on galaxies, it is much more difficult, however, to unambiguously photometrically confirm the presence of a bar in an edge-on galaxy. This problem was simplified when Kuijken & Merrifield (1995) and Merrifield & Kuijken (1999) demonstrated that bars in edge-on galaxies could be detected kinematically from features like parallelograms and figures-of-eight in the position-velocity diagrams. Subsequent observations and simulations (e.g. Bureau & Freeman 1999; Bureau & Athanassoula 1999; Athanassoula & Bureau 1999; Chung & Bureau 2004; Bureau & Athanassoula 2005) have confirmed the relationship between B/PS bulges, complex kinematics, and bars.

We have obtained the optical long-slit spectrum and SparsePak Integral Field Unit (IFU) velocity field, as well as optical and near-IR images, of NGC 2683, an isolated, nearly edge-on Sb galaxy with a B/PS bulge. NGC 2683 is highly inclined; Funes et al. (2002) report an inclination of 78°, while others suggest a *minimum* inclination of 80° (e.g. Barbon et al. 1975; Broeils et al. 1994). The complex kinematic and photometric features of the data are suggestive of a bar in the galaxy. Although previous authors have observed NGC 2683 and linked its complex velocity structure and bulge shape with a bar, there has been little discussion about the bar orientation.

In this paper we present our spectroscopic and photometric observations as evidence that NGC 2683 contains a bar that is 6° on the sky away from the galaxy major axis. In § 2 we review the data for NGC 2683 in the literature. Our new observations and data reduction are discussed in § 3. We present the spectroscopic data in § 4 and the photometric data in § 5. We describe in each section how these data support the hypothesis that a bar is present in the galaxy, and use the features of the kinematic and photometric signatures to constrain the orientation of the bar. The results for NGC 2683 are compared in § 6 with the results for M31 by Athanassoula & Beaton (2006). A comparison to M31 is insightful, as it has photometric and kinematic characteristics, as well as an inclination, that are similar to NGC 2683. Finally, a summary is presented in § 7.

2. PREVIOUS OBSERVATIONS

Because of its prominent boxy/peanut-shaped bulge and interesting kinematics, NGC 2683 has been a well-

---

Electronic address: kuzio@uci.edu
Electronic address: mzagursk@umd.edu
Electronic address: ssm@astro.umd.edu

[1] NSF Astronomy and Astrophysics Postdoctoral Fellow

studied object. In 1974, de Vaucouleurs classified the bulge as peanut-shaped. Ford, Rubin, & Roberts (1971) obtained a long-slit spectrum of the galaxy and noted that outside of the nucleus, the [N II]λ6584 emission was fainter than the Hα emission, whereas inside the nucleus, it was brighter than the Hα emission. Barbon & Capaccioli (1975) presented B-band photometry and optical emission line spectroscopy. Based on the galaxy image, they found the bulge to be peanut-shaped and the dust-obscured NW side of the galaxy to be the near side. The spectroscopic data showed trailing spiral arms, a [N II]/Hα ratio in the outer parts of the galaxy consistent with what is seen in HII regions ([N II] emission that is fainter than Hα emission), and strong evidence for deviations from circular motions. de Souza & dos Anjos (1987) classified the bulge+disk shapes of 72 galaxies and categorized NGC 2683 as a BS-II galaxy: a system in which the disk and bulge components are not sharply distinct and the bulge is an elongated ellipsoid that is sometimes rectangular. An HI rotation curve of the galaxy was presented by Casertano & van Gorkom (1991), and noncircular motions were noted. J- and K-band photometry, as well as *(J-K)* color, eccentricity, position angle and cos 4θ profiles as functions of radius were presented by Shaw (1993), as were models of the observed luminosity distribution. Rubin (1993) found the Hα and [N II] emission to show multi-valued, figure-of-eight velocity structure in the inner 60″ of the galaxy. Light from bulge stars or foreground gas warping out of the galaxy plane and into the line-of-sight were suggested as possible explanations for the observed complex velocity structure. An HI position-velocity map of NGC 2683 was presented by Broeils & van Woerden (1994).

The link between boxy bulges and bars was investigated by Merrifield & Kuijken (1999) using a sample of 10 galaxies, including NGC 2683. They found that the emission line kinematics of galaxies with boxy bulges show complex velocity structure; the position-velocity diagrams can be described as being X-shaped or containing features similar to figures-of-eight or parallelograms. The complex kinematics of NGC 2683 were also observed by Pompei & Terndrup (1999) who noted the presence of a counter-rotating stellar system and two gas components, one of which was rotating in the same sense as the stellar component, and the other rotating in the opposite direction. A nuclear bar close to the minor axis or a merger event were two scenarios given to explain the counter-rotation. Additionally, Pompei & Terndrup (1999) observed the bulge isophotes to be boxy inside 50″. Optical and NIR photometry also led Lütticke, Dettmar, & Pohlen (2000a,b) to classify the bulge of NGC 2683 as box-shaped. Stellar and ionized gas velocity curves as well as velocity dispersions were presented by Vega Beltrán et al. (2001). They, too, detected kinematically distinct stellar and gas components, but remarked that they were unable to resolve the fast and slow rotating components in the gas. Funes et al. (2002) presented a position-velocity diagram for NGC 2683 derived from Hα, [N II]λ6584, and [O III]λ5007 emission. Due to the low S/N of their data, the figure-of-eight shape in the position-velocity diagram was faint, but they did observe two spatially distinct gas components.

3. NEW OBSERVATIONS AND DATA REDUCTION

3.1. *Spectroscopy*

We observed NGC 2683 with the RC Spectrograph on the Kitt Peak National Observatory (KPNO) 4-meter telescope during the nights of 2007 October 16 and 18. We used the T2KB CCD with the 860 line mm^{-1} grating in second order, centered near Hα. The slit width was 1.5″, giving $\sim$ 1.0 Å spectral resolution and a spatial scale of 0.69″ pixel^{-1}. We centered the slit on a nearby bright star and then offset to the optical center of the galaxy. Two 600 s exposures were taken with the slit aligned along the major axis of the galaxy (position angle = 41.5°). A HeNeAr lamp was observed before and after each science exposure to provide wavelength calibration.

We also observed NGC 2683 with the SparsePak IFU on the 3.5-meter WIYN [2] telescope at KPNO on the night of 18 February 2009. SparsePak is a 70″ × 70″ fixed array of 82 5″ diameter fibers. We used the STA1 CCD with the 316@63.4 grating in eighth order, centered near Hα, giving a 40 km s^{-1} velocity resolution. The SparsePak array was aligned with the major axis of the galaxy and five pointings were used to cover the entire length of the galaxy. Each exposure was 1200 s, and two exposures were taken at each pointing. A ThAr lamp was observed to provide wavelength calibration.

The spectral data were reduced using standard reduction routines in IRAF[3]. The data were bias-subtracted and flattened. The IRAF task `dohydra` was used to extract the IFU spectra. The galaxy spectra were wavelength-calibrated using a wavelength solution created from the observations of the comparison HeNeAr and ThAr lamps. To increase the signal-to-noise and remove cosmic rays, the two galaxy frames per pointing were combined. In general, the galactic emission lines in the spectra are much stronger than the night-sky emission lines, and the night-sky lines bracket, rather than overlap, the galaxy lines. Sky subtraction was not performed for either data set and we subsequently used the night-sky emission lines as the reference wavelengths (Osterbrock et al. 1996) by which the velocities of the galactic emission lines were measured. The velocities were measured by fitting Gaussians to both the sky lines and the five galactic emission lines of interest: Hα, [N II]λ6548, [N II]λ6584, [S II]λ6717, [S II]λ6731. There was less scatter between the measured galactic emission line velocities when using the night-sky calibration than either the HeNeAr or ThAr calibrations.

3.2. *Photometry*

The galaxy was also imaged at the KPNO 2.1-meter telescope during the night of 2007 March 17. The galaxy was imaged in B, V, R, and I, with total exposure times of 600 s, 600 s, 300 s, and 300 s, respectively. Two exposures were taken in each band to correct for cosmic rays. The T2KB CCD was used, and the spatial resolution was 0.305″ pixel^{-1}. These data were taken under

---

[2] Based on observations obtained at the WIYN Observatory. The WIYN Observatory is a joint facility of the University of Wisconsin-Madison, Indiana University, Yale University, and the National Optical Astronomy Observatory.

[3] IRAF is distributed by the National Optical Astronomy Observatory, which is operated by the Association of Universities for Research in Astronomy (AURA), Inc., under agreement with the National Science Foundation.

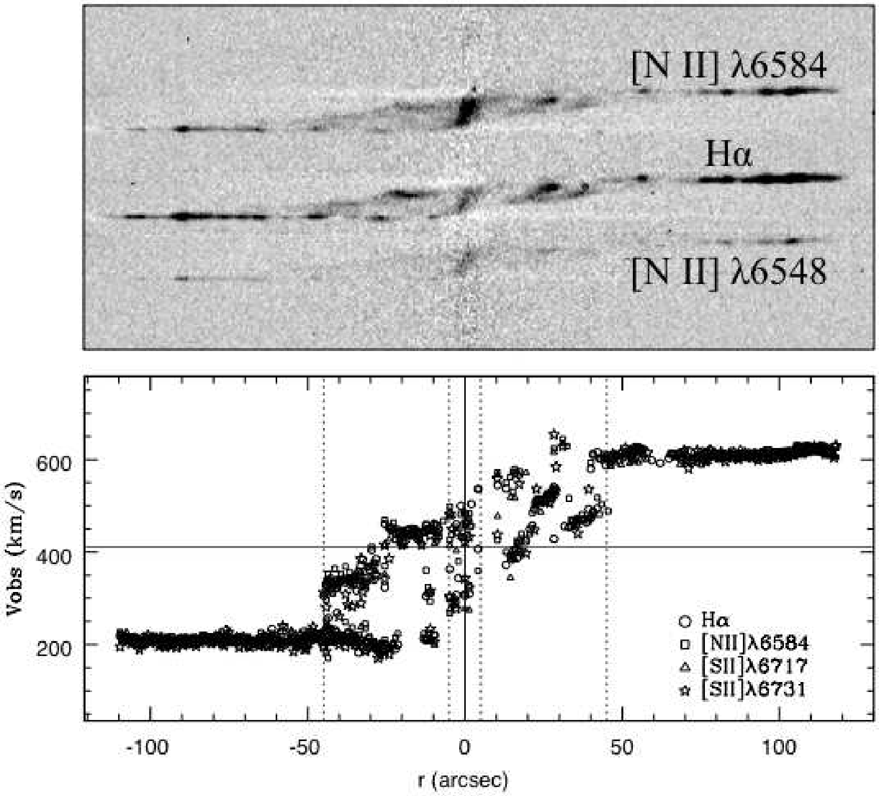

FIG. 1.— *Top:* Observed Hα and [N II] region of the long-slit position-velocity diagram. The emission traces two parallelogram shapes: an outer parallelogram extending to about ±45″, and a compact, inner parallelogram extending to about ±5″. *Bottom:* Observed velocities of the Hα, [N II]λ6584, [S II]λ6717, and [S II]λ6731 emission lines. The error on the velocity at a given position is equal to the scatter in the measured velocities of the observed emission lines, ~10 km s^{-1}. At radii $\lesssim 45''$, the velocities are multi-valued. The measured velocities occupy the two forbidden quadrants of the PVD; there is red-shifted emission on the blue-shifted side of the galaxy (upper left quadrant) and blue-shifted emission on the red-shifted side of the galaxy (lower right quadrant).

non-photometric conditions. The optical broad-band images were bias-subtracted, flattened, and combined using standard IRAF routines. 2MASS *J*- and *K*-band images of NGC 2683 are also available, and were downloaded from the on-line 2MASS catalog (Skrutskie et al. 2006).

4. KINEMATIC SIGNATURES

4.1. *Long-slit Position Velocity Diagram*

In Figure 1 we show the observed Hα and [N II]λλ6548, 6584 region of the long-slit position-velocity diagram (PVD) of NGC 2683. The PVD shows complex structure out to radii of $\sim 45''$, almost half of its entire length. The Hα and [N II] emission (as well as the [S II]λ6717 and [S II]λ6731 emission that are not shown) trace a parallelogram shape extending to $\sim 45''$ on each side. The edges of this region are relatively bright compared to the faint interior emission. At radii $\lesssim 45''$, the velocities are double, sometimes triple, valued. The maximum velocity reached is comparable to the velocities reached in the outer parts of the galaxy. The parallelogram velocities are seen to populate the "forbidden" quadrants of the PVD; there are red-shifted velocities on the blue-shifted side of the galaxy and vice versa.

There is also a second parallelogram feature seen in the PVD. In approximately the inner $\pm\,5''$ there is a steeper and more compact parallelogram that is brighter in the [N II]λ6584 emission than Hα. The velocities reached in this region do not exceed the velocities in the more extended parallelogram or those of the outer disk, and there is a smooth transition between the compact, inner and extended, outer parallelogram-shaped features.

This complex "figure-of-eight" PVD can be explained by the presence of a bar in the galaxy. In a series of papers, Bureau & Athanassoula (1999, hereafter BA99), Athanassoula & Bureau (1999, hereafter AB99), and Bureau & Athanassoula (2005, hereafter BA05) used simulations of edge-on ($i = 90°$) galaxies to demonstrate that features in PVDs like those shown in Figure 1 can be explained by gas (and stars) moving in the x_1 and x_2 families of periodic orbits of barred potentials. Each of these orbit families produces unique signatures in the PVD and, by virtue of the orientations of the orbits with respect to the bar, the appearance of the PVD features can be used to put constraints on the position angle of the bar.

BA99, AB99, and BA05 showed that in edge-on galaxies x_1 orbits produce extended features in the PVD that range from bow tie-shaped to parallelogram-shaped depending on the orientation of the bar with respect to the observer's line-of-sight (see Figure 2). The x_1 orbits are elongated parallel to the major axis of the bar, so that when the bar is viewed end-on, the line-of-sight is parallel to the major axis of both the bar and x_1 orbits. Viewed at this angle, the "fast" parts of the elongated x_1 orbits are pointing directly toward or away from the observer and very high radial velocities at small projected

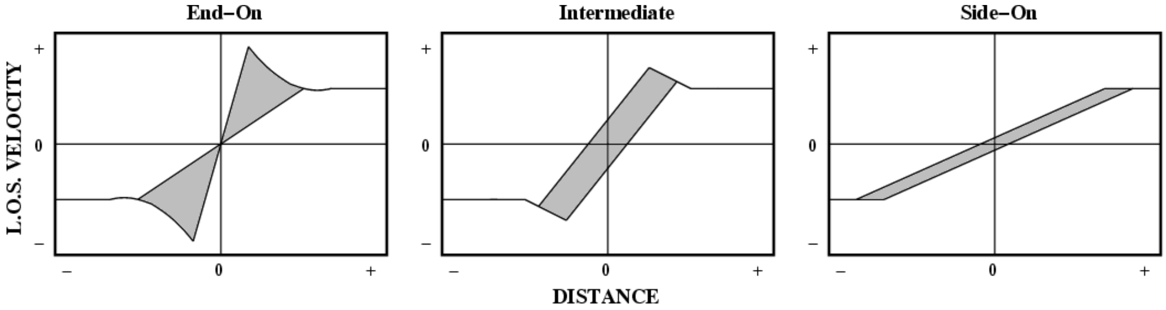

FIG. 2.— Schematic representation of the shape of the position-velocity diagram produced by x_1 orbits for different lines of sight. The major axes of both the bar and x_1 orbits are parallel to the observer's line-of-sight when the bar is viewed end-on, and are perpendicular to the observer's line-of-sight when the bar is viewed side-on.

distances are observed. This produces a bow tie-shaped feature in the PVD.

When the bar is viewed side-on, the elongated axis of the x_1 orbits is perpendicular to the line-of-sight. The "slow" parts of the x_1 orbits are thus pointing directly toward or away from the observer, and as a result, much lower radial velocities are observed. In addition, because the long axis of the orbits is across the line-of-sight, these observed velocities will extend to larger projected distances than when the bar (and x_1 orbits) is viewed end-on. The resulting feature in the PVD is therefore a relatively thin, diagonal band of velocities extending to large projected distances.

When the bar in an edge-on galaxy is not viewed directly end-on or side-on, the PVD will contain a parallelogram-shaped feature with velocities appearing in the "forbidden" quadrants. This velocity structure arises because the orbits are elongated and not circular. The line-of-sight does not fall along either the major axis or minor axis of the orbits. Thus, if they are viewed at an angle other than end-on or side-on, the positions along the orbits where the tangential velocity is greatest (and radial velocity is zero) will be offset from the center. This means that the velocities transition from being blue-shifted to red-shifted, and vice versa, at radii greater than zero. This leads to red(blue)-shifted velocities being observed on the blue(red)-shifted side of the galaxy, thus falling in the "forbidden" quadrants. The closer the bar is to end-on, the sharper and more peaked the parallelogram is at small projected radii (and the more it looks like a bow tie). The interior of these PVDs also tend to be brighter than the edges. As the bar angles closer to side-on, the corners of the parallelogram round out and the parallelogram becomes thinner as it extends to larger projected distances and rises to lower radial velocities.

In the observed PVD of NGC 2683, the broad ($\pm 45''$) parallelogram shape corresponds to the x_1 feature. The simulated PVDs of BA99, AB99, and BA05 can serve only as a *guide* to the bar orientation in our galaxy because (a) NGC 2683 is not exactly edge-on ($i \gtrsim 78°$), and (b) the models are not tailored to specifically match NGC 2683 (bar strength, pattern speed, mass distribution, etc). With that caveat in mind, both the bright emission along the edges of the x_1 parallelogram and a lack of clear central peaks suggest that the bar is oriented at an intermediate angle (perhaps between 10° and 45°) on the sky away from the galaxy major axis and therefore viewed closer to side-on than end-on.

At the center of the observed PVD of NGC 2683 is the signature of the x_2 orbits: a compact feature that is brighter in [N II] emission than Hα emission (Figure 1; see also Ford, Rubin, & Roberts 1971). This relatively large [N II] emission may be caused by the shocks that develop at the transition between the x_1 and x_2 orbits (Baldwin, Phillips, & Terlevich 1981; Dopita & Sutherland 1996; AB99), as well as the AGN that is known to be at the center of NGC 2683 (Irwin, Saikia, & English 2000). Without additional diagnostic emission lines such as [O I] or [O III], we cannot say for certain that it is the AGN rather than shocks that is causing the bright [N II] emission. It is not uncommon for barred galaxies to host AGN. Philips, Charles, & Baldwin (1983) observed a number of relatively face-on SB galaxies with large [N II]/Hα ratios and confirmed the presence of active nuclei. Knapen, Shlosman, & Peletier (2000) have also found that galaxies with active centers are more often barred (79%) than galaxies without active nuclei (59%) (see also Laurikainen, Salo, & Buta 2004).

The x_2 orbits are elongated perpendicular to the bar (making them also perpendicular to the x_1 orbits) and are less radially extended than the x_1 orbits. Because the major axes of the x_2 and x_1 orbits are perpendicular, when one orbit family reaches its maximum radial velocity, the other is at its minimum. Thus, the radial velocities of the x_2 orbits peak when the bar is viewed side-on and are lowest when the bar is viewed end-on.

Rather than using the shape of the x_2 feature in the PVD, AB99 advocate the ratio of the maximum observed radial velocity of the x_2 orbits to the maximum velocity observed in the outer parts of the galaxy (V_{x2}/V_{disk}) as the best measure of bar viewing angle. When the bar is viewed close to end-on, the maximum velocity of the x_2 orbits will be low compared to the outer disk (the line-of-sight is perpendicular to the elongated axis of the x_2 orbits and the "slow" parts of the orbit are observed); $V_{x2}/V_{disk} \lesssim 1$ in this case. The "fast" parts of the x_2 orbits are observed when the bar is viewed side-on; it therefore follows that $V_{x2}/V_{disk} \gtrsim 1$ in this orientation. In NGC 2683, we find that $V_{x2}/V_{disk} \approx 0.6$. This value of V_{x2}/V_{disk} suggests that the bar is viewed nearer to end-on than side-on.

This result contrasts with the other indicators we have, both photometric and kinematic, that suggest a more side-on orientation. The V_{x2}/V_{disk} indicator advocated by AB99 appears to be one of the more promising indicators of bar orientation. However, it must depend on the details of the disk mass distribution. Some galaxies have a distinct peak in their rotation curves before declining to a flat level while others rise continuously. Consequently,

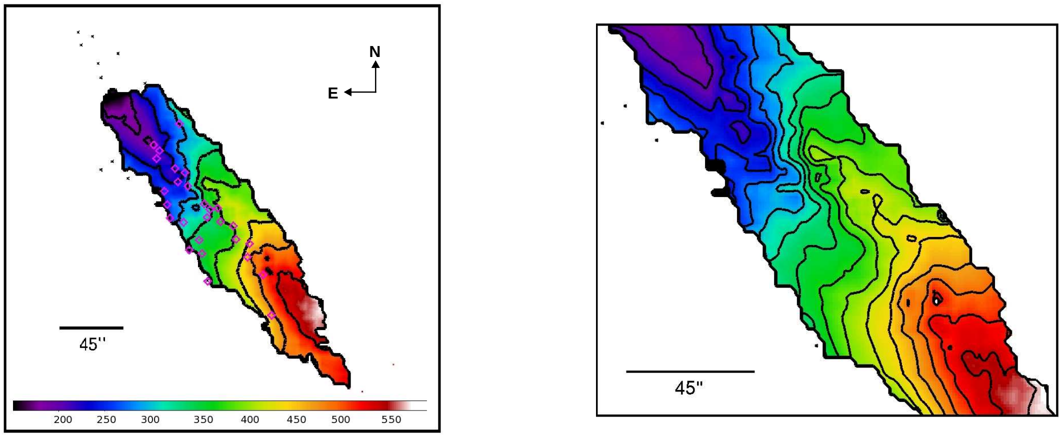

FIG. 3.— Observed Hα SparsePak velocity field of NGC 2683. The entire velocity field is shown in the left panel while a zoomed-in version with the same color/velocity scale is shown on the right. The galaxy major and minor kinematic axes are clearly skewed from perpendicular. Diamonds in the left panel indicate fibers containing multi-valued Hα velocities. In the full velocity field, isovelocity contours are spaced in 50 km s^{-1} intervals. To highlight the twist of the minor axis, the isovelocity contours are spaced in 25 km s^{-1} intervals in the right panel. In both panels, a 45$''$ line indicates the radius of the parallelogram in the long-slit PVD in Figure 1. North is up and East is to the left. (A color version of this figure is available in the online journal.)

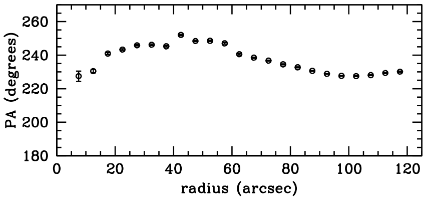

FIG. 4.— Variation in position angle (PA) across the velocity field.

V_{disk} of this particular galaxy may not correspond well to that of the AB99 model. More generally, it may be an indication that we still do not have a complete understanding of the complex kinematics in NGC 2683.

4.2. *SparsePak IFU Velocity Field*

In Figure 3 we show the observed Hα SparsePak velocity field of NGC 2683. The major and minor kinematic axes are not perpendicular and there is an S-shaped twist to the minor axis. These are characteristic of velocity fields with oval distortions or bars (e.g. Bosma 1981). Similar S-shaped velocity fields can be seen in observations of more face-on barred galaxies such as NGC 6300 (i=52°, Buta 1987) and NGC 5383 (i=50°, Peterson et al. 1978). As in the long-slit spectrum, double and triple-valued Hα velocities (as well as [N II] and [S II] velocities) are detected in some of the IFU fibers. The multi-valued velocities are more striking in the long-slit spectrum than in the velocity field.

Analysis of the velocity field with the tilted-ring fitting program `ROTCUR` (Teuben 1995; Begeman 1989) shows that the position angle (PA) varies by $\sim$ 25° across the velocity field, with the largest deviation from the PA of the outer galaxy occuring at $\sim 45''$, the length of the x_1 parallelogram in the long-slit PVD (see Figure 4). If we assume that there should be a steep velocity gradient (i.e. the isovelocity contours bunch up) across the bar and that the central minor axis velocity contours run along the length of the bar, then the center of the velocity field qualitatively indicates (visually) that the bar is angled not far (perhaps $\sim$ 15°) from the galaxy major axis on the sky, running from northeast to southwest. This is supported by the change in PA determined by `ROTCUR`; the bar is a maximum of 25° from the major axis. This angle implies that the bar is viewed more side-on than end-on, in agreement with the constraints from the parallelogram in the long-slit PVD produced by x_1 orbits.

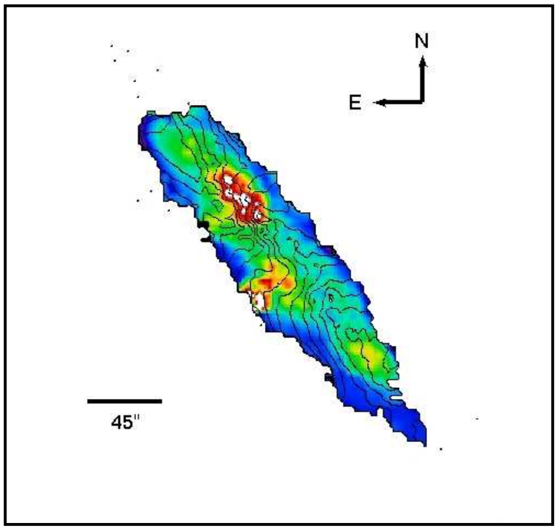

FIG. 5.— Hα image of NGC 2683 created from the SparsePak IFU data with velocity contours overlaid. The brightest and most concentrated Hα emission coincides with the ends of the bar. (A color version of this figure is available in the online journal.)

In Figure 5 we show the Hα image of NGC 2683 constructed from the IFU data with isovelocity contours from the velocity field overplotted. We find that while there is diffuse emission throughout the galaxy, the brightest concentrations of emission coincide with the bends in the S-shape (the ends of the bar). The NE (upper) end of the bar is slightly brighter than the SW (lower) end and there is no strong emission along the length of the bar.

Strong Hα emission at the bar ends and relatively weak emission along its length has also been seen in the relatively face-on galaxies NGC 1530 (Zurita et al. 2004), NGC 5383 (Sheth et al. 2000), and NGC 6300 and NGC 1433 (Buta et al. 2001). Similar to what is seen in

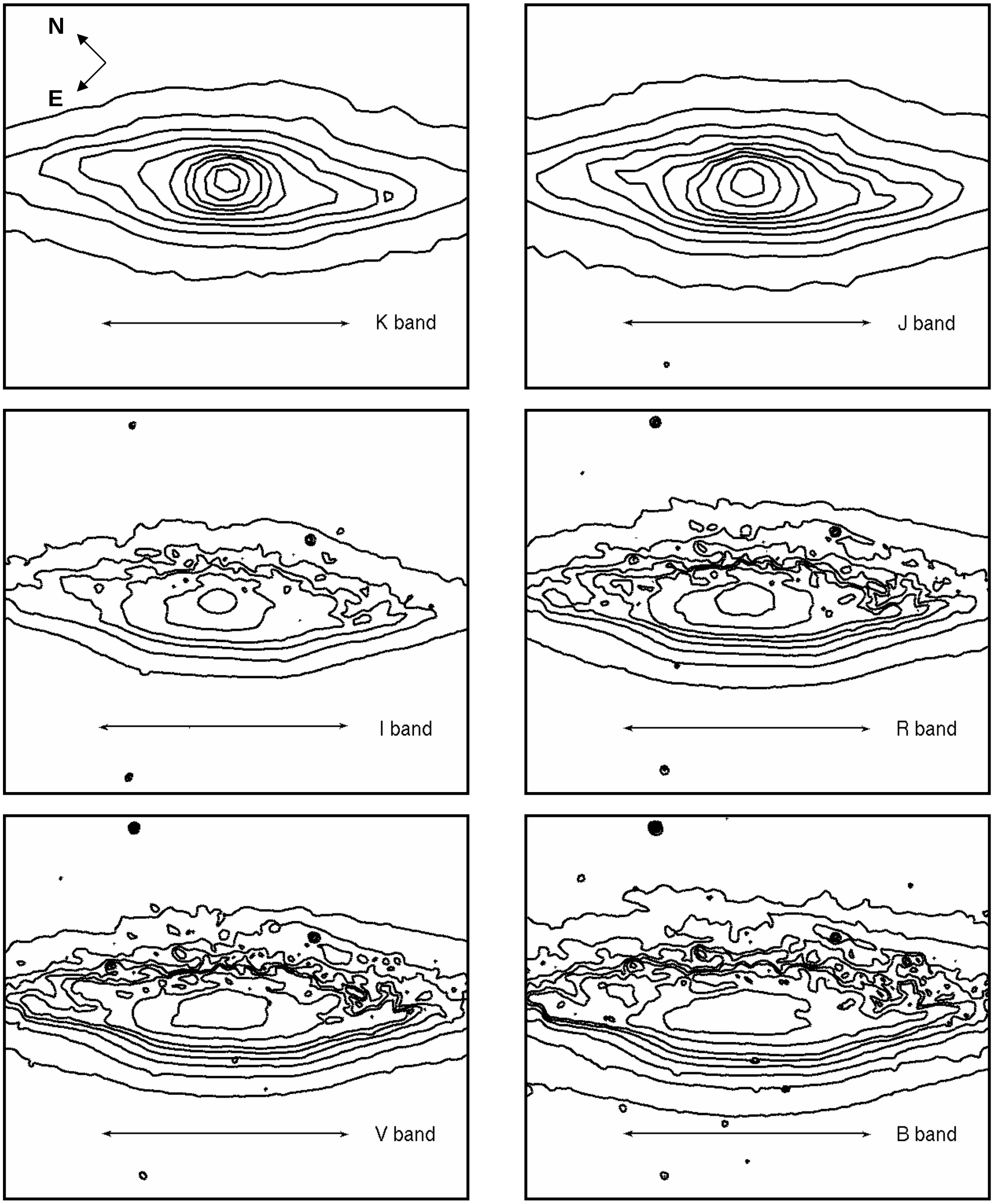

Fig. 6.— Contour plots of the bulge region of NGC 2683, ordered by wavelength from longest to shortest. For comparison, isophotes are at the same relative levels for each frame. The bulge of NGC 2683 is boxy: the isophotes are parallel to the major axis and do not show a pinch along the minor axis. The arrows indicate ±45″, the length of the x_1 extended parallelogram feature in the position-velocity diagram. North is towards the upper left corner, East to the lower left corner. In the optical images there is significant dust on the northwest side of the galaxy.

NGC 2683, Zurita et al. (2004) found that the brightest Hα emission in NGC 1530 coincides with the regions of lowest velocity gradient perpendicular to the bar (regions were the isovelocity contours are not bunched up).

5. PHOTOMETRIC SIGNATURES

Boxy/peanut-shaped bulges in edge-on galaxies have been shown to correlate with the presence of a bar (e.g. Combes & Sanders 1981; Combes et al 1990; Bureau & Freeman 1999). It is thought that these bulge shapes are a result of a bar that has buckled and thickened due to vertical instabilities (e.g. Combes et al 1990). Depending on the bar strength and the orientation of the bar with respect to the line-of-sight, the bulge may look round (the bar is viewed end-on), boxy (the bar is viewed at an intermediate angle), or peanut-shaped (the bar is viewed side-on) (e.g. Chung & Bureau 2004; Bureau & Athanassoula 2005).

In Figure 6, we show contour plots of the bulge region of the *B, V, R, I, J,* and *K* images of

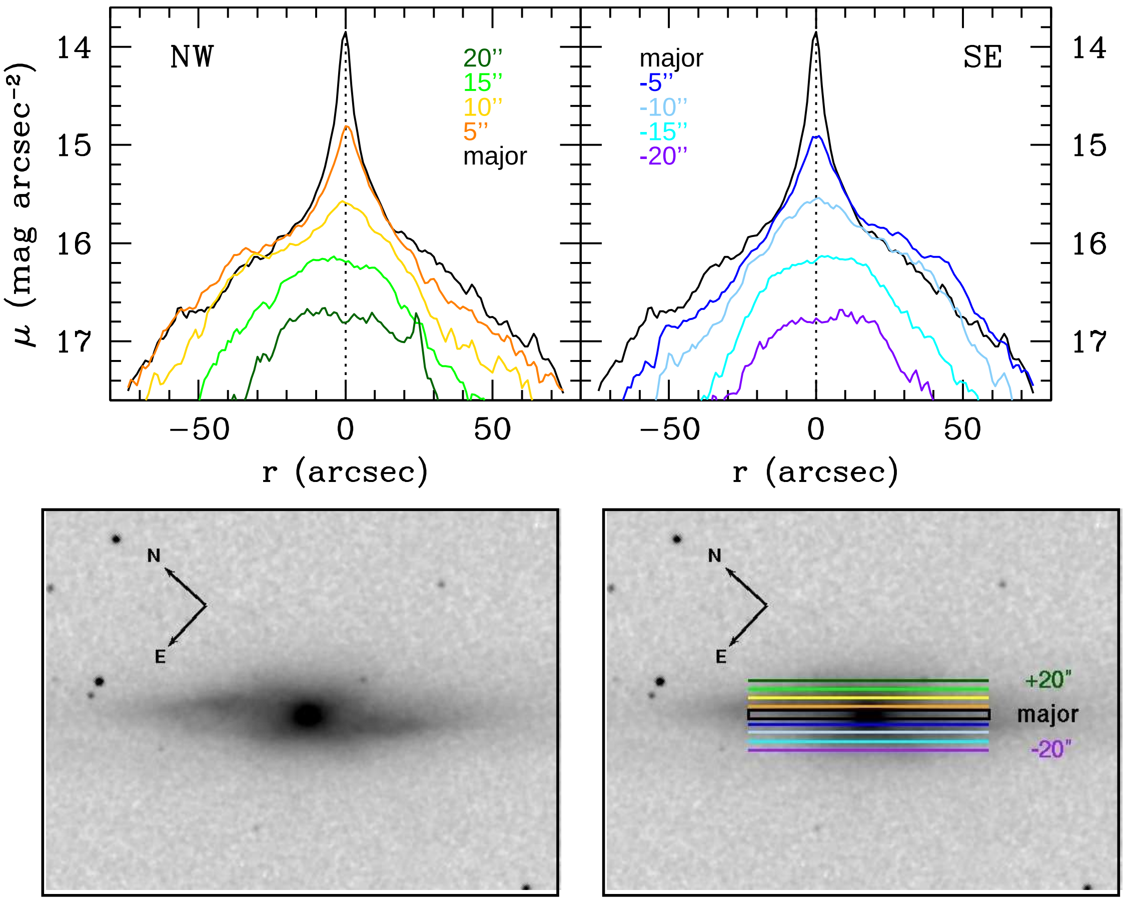

Fig. 7.— K-band surface brightness measured along $5'' \times 140''$ slits positioned parallel to the major axis. There is an enhancement in the light profile in the N−S direction, suggesting the presence of a bar at a mild angle with respect to the major axis. (A color version of this figure is available in the online journal.)

NGC 2683. Lütticke, Dettmar, & Pohlen (2000a) define peanut-shaped bulges as having isophotes that pinch inwards along the minor axis on both sides of the galaxy major axis, and boxy bulges as having isophotes that remain parallel to the major axis. Applying these definitions to Figure 6, it is clear that the bulge of NGC 2683 is boxy. This is most easily seen in the K-band image of the galaxy where the obscuration from dust is at a minimum. On both sides of the major axis, the isophotes are parallel and remain flat as they cross the minor axis. Even as the galaxy is viewed through progressively bluer filters and the effects of dust on the northwest side of the galaxy become more severe, the isophotes on the less-obscured side of the galaxy do not show signs of pinching along the minor axis that are characteristic of a peanut-shaped bulge. The classification of the bulge shape is independent of wavelength (see also Lütticke, Dettmar, & Pohlen 2000a).

Two of us (RKD and SSM) made independent ellipse fits with different fitting routines (`ellipse` in IRAF and ARCHANGEL (Schombert 2007)). While these ellipse fits are broadly consistent, they give slightly different results for the boxiness/pointiness parameter b_4. Thorough examination of the images and residuals of the fits shows that this can be traced to isophotes that are both boxy and pointy. This is most apparent in the J and K-band images in Figure 6. Along the minor axis of the bulge, the isophotes are flatter than a pure ellipse, indicating a boxy bulge. Along the major axis, the isophotes become pointy, so that the entire isophote shape is both pointy and boxy. We interpret the pointiness to be due to the bar itself extending out into the disk; see Figures 7 and 8. The length of the boxy region, corresponding to the thick inner part of the bar, is about $\pm 23''$ in the K-band. The pointy isophotes extend to roughly $\pm 54''$ and correspond to the thin outer part of the bar.

It is not uncommon for barred galaxies to have features that connect to the ends of the bar such as ansae ("handles") or rings (e.g. Martinez-Valpuesta, Knapen, & Buta 2007; Buta et al. 2001). Because NGC 2683 is so highly inclined, it is difficult to determine if these structures are also present.

The boxy bulge shape of NGC 2683 indicates that the bar is not so strong as to induce the pinched isophotes of a peanut and that the bar is positioned at an intermediate viewing angle. To determine the general orientation of the bar, we plot in Figure 7 the observed surface brightness measured along $5'' \times 140''$ slits positioned parallel to the galaxy major axis. We find that the surface brightness profiles are asymmetric around the minor axis. Specifically, in the slices above the major axis (the northwest slices), there is a "hump" in the profile indicating excess light to the left (north) of the galaxy minor axis and in the slices below the major axis (the southeast

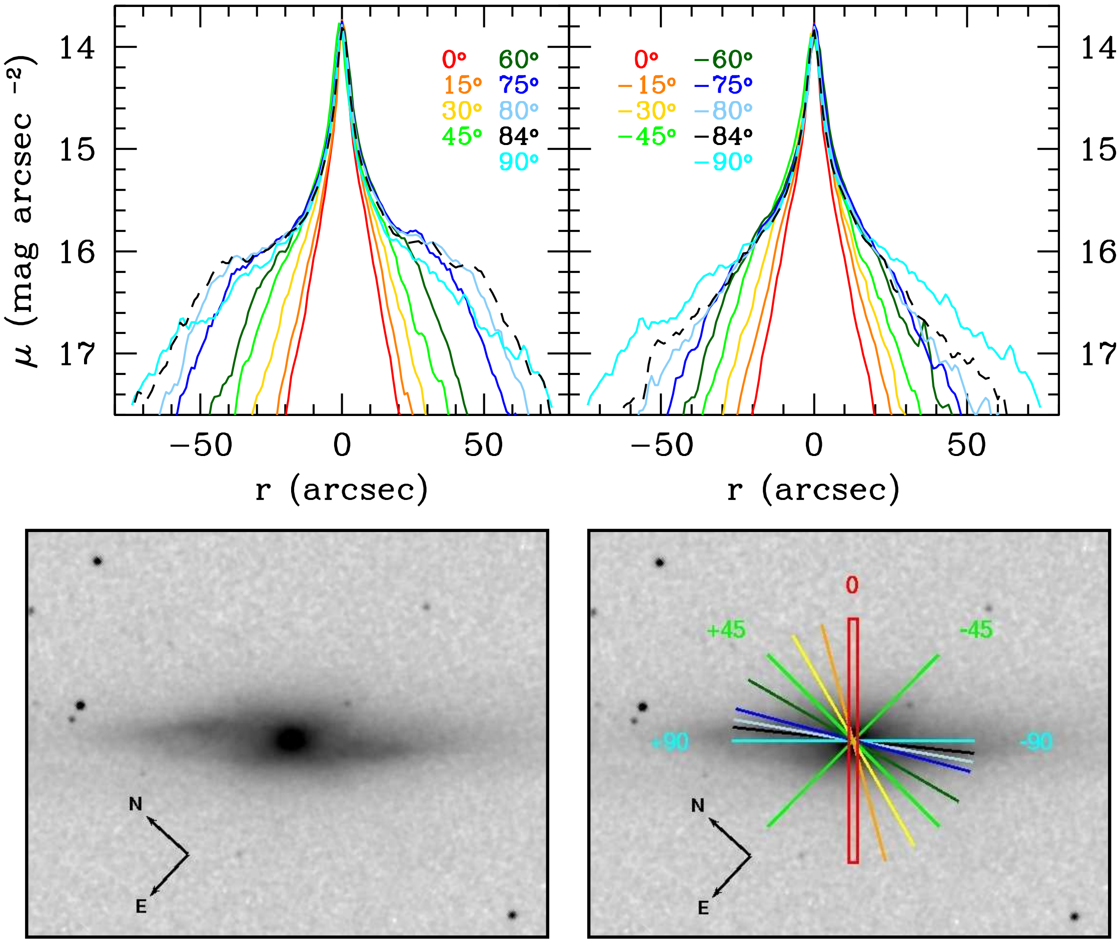

FIG. 8.— K-band surface brightness measured along $5'' \times 140''$ slits oriented at different position angles. There is an enhancement in the light above the level of the major axis along the +84° slit. (A color version of this figure is available in the online journal.)

slices), the ehancement in the light is to the right (south) of the galaxy minor axis. We interpret this asymmetry in the light profiles as an indication that the bar is aligned in a N-S direction, consistent with the orientation derived from the SparsePak velocity field. Consistent with the approximate lengths of the boxy and pointy isophote regions, the excess light begins around $\pm\, 20''{-}25''$, peaks around $45''$, and drops off between $50''$ and $60''$. Based on the photometry, we estimate the length of the bar to be $\sim 55''$.

In Figure 8, we confirm this N-S orientation by plotting surface brightness profiles along slits oriented at different position angles. We define 0° as the minor axis and 90° as the major axis. There is an enhancement in the light along the slits rotated counterclockwise (positive angles) from the galaxy minor axis. The humps in the profile reach a maximum above the level of the light along the major axis at a position angle of +84° from the minor axis (or, equivalently, 6° from the major axis). This angle coincides with the asymmetric, elongated isophotes seen most clearly in the K-band image. In agreement with the kinematic data, the humps in the surface brightness profiles extend to $\sim 45''{-}50''$. Based on the photometric signatures, we conclude that the bar is oriented $\sim 6°$ from the galaxy major axis on the sky, running from north to south.

6. COMPARISON TO M31

It is instructive to compare the observations of NGC 2683 with observations of other galaxies having similar inclinations ($i \gtrsim 78°$) and bar orientations ($\varphi_{phot} \sim 6°$, $\varphi_{kin} \sim 10° - 25°$). One such example is M31. Athanassoula & Beaton (2006) recently used kinematic and photometric data to argue for the presence of a bar in the galaxy (see also Lindblad 1956; Stark & Binney 1994). They find that M31 ($i = 77°$) contains a medium-strength bar that is on the order of $\varphi \sim 7°$ on the sky away from the galaxy major axis ($\mathrm{PA}_{disk} = 38°$, $\mathrm{PA}_{bar} \sim 45°$).

The observed PVDs of NGC 2683 and M31 show similar complex kinematics. The observed HI PVD of M31 (their Figure 9) is more bow tie-shaped than the long-slit Hα PVD of NGC 2683. As discussed in §4.1, in edge-on galaxies, the PVD appears more bow tie-like as the bar angles farther away from the major axis. Taken at face value, the observed PVDs would therefore suggest that the bar in M31 is seen more end-on than the bar in NGC 2683. The simulations described in §4.1, however, are *ideal* and in reality, the observed kinematics are highly influenced by physical conditions in the galaxy, such as the presence of dust or the density of the gas. Without further modeling, we cannot say whether the differences in the PVDs originate from these physical differences or from different bar orientations or some combination of both.

The isophotes seen in the images of M31 (their Figure 2) are similar to the isophotes of the K-band image of NGC 2683; the isophotes are boxy rather than pinched in a peanut shape. Based on isophote shapes in N-body simulations tailored to the orientation of M31, they argue that the absence of peanut-shaped isophotes means the bar is not a strong bar (see also Lütticke, Dettmar, & Pohlen 2000b; Athanassoula & Misiriotis 2002). By this standard, the bar in NGC 2683 is not strong. Similar to NGC 2683, M31 has elongated isophotes that are angled away from the major axis and indicate the PA of the bar. Additionally, they find similar asymmetric enhancements in the light profile in slits parallel to the major axis (their Figures 5 and 6).

It is encouraging that there are so many similarities between the observations of these two galaxies. Bars in nearly edge-on galaxies cannot be unambiguously visually confirmed as such, but strong evidence for their presence comes from the comparison of observed kinematic and photometric signatures to the results of numerical simulations. That simulations are consistent with numerous observed galaxies increases our confidence in using bars to explain boxy/PS bulges and figure-of-eight PVDs.

7. SUMMARY

We have presented new spectroscopic and photometric observations of the near edge-on spiral galaxy NGC 2683. The long-slit PVD displays a complex, figure-of-eight distribution of velocities, and the SparsePak IFU velocity field shows characteristics of an oval distortion. Isophotes in optical and near-IR images of the galaxy are boxy. We find an asymmetric enhancement in the light profile in slits placed parallel to, and offset from, the major axis.

We argue that the kinematic and photometric signatures are evidence that the galaxy hosts a bar. We find that the data support a bar that is viewed closer to side-on than end-on (i.e. closer to the galaxy major axis than the minor axis). Based on kinematic and photometric constraints, we determine that the bar is 6° away from the major axis on the sky. Our results are consistent with previous observations of NGC 2683 in the literature, as well as recent results for M31, and add to the growing body of evidence linking B/PS bulges and complex PVDs with bars in edge-on galaxies.

We would like to thank the referee for helpful comments. R.K.D. is supported by an NSF Astronomy & Astrophysics Postdoctoral Fellowship under award AST 07-02496. S.S.M. and M.J.Z. are supported by NSF grant AST 05-05956. We would like to thank L. Athanassoula for helpful conversations. R.K.D. would also like to thank Brian Marsteller and Misty Bentz for useful discussions. This publication makes use of data products from the Two Micron All Sky Survey, which is a joint project of the University of Massachusetts and the Infrared Processing and Analysis Center/California Institute of Technology, funded by the National Aeronautics and Space Administration and the National Science Foundation.

REFERENCES

Athanassoula, E. & Beaton, R. L. 2006, MNRAS, 370, 1499
Athanassoula, E. & Bureau, M. 1999, ApJ, 522, 699 (AB99)
Athanassoula, E. & Misiriotis, A. 2002, MNRAS, 330, 35
Baldwin, J. A., Phillips, M. M., & Terlevich, R. 1981, PASP, 93, 5
Barbon, R. & Capaccioli, M. 1975, A&A, 42, 221
Begeman, K. 1989, A&A, 223, 47
Binney, J., & Petrou, M. 1985, MNRAS, 214, 449
Bosma, A. 1981, AJ, 86, 1825
Broeils, A. H., & van Woerden, H. 1994, A&A, 107, 129
Bureau, M. & Athanassoula, E. 1999, ApJ, 522, 686 (BA99)
Bureau, M. & Athanassoula, E. 1999, ApJ, 626, 159 (BA05)
Bureau, M. & Freeman, K. C. 1999, AJ, 118, 126
Buta, R. 1987, ApJS, 64, 383
Buta, R., Ryder, S. D., Madsen, G. J., Wesson, K., Crocker, D. A., & Combes, F. 2001, AJ, 121, 225
Casertano, S. & van Gorkom, J. H. 1991, AJ, 101, 1231
Chung, A., & Bureau, M. 2004, AJ, 127, 3192
Combes, F. & Sanders, R. H. 1981, A&A, 96, 164
Combes, F., Debbasch, F., Friedli, D., & Pfenniger, D. 1990, A&A, 233, 82
de Souza, R. E., & dos Anjos, S. 1987, A&A, 70, 465
de Vaucouleurs, G. 1974, in IAU Symp. 58, Formation and Dynamics of Galaxies, ed. J. R. Shakeshaft (Reidel: Dordrecht), 335
Dopita, M. A., & Sutherland, R. S. 1996, ApJS, 102, 161
Eskridge, P. B., Frogel, J. A., Pogge, R. W., Quillen, A. C., Davie, R. L., DePoy, D. L., Houdashelt, M. L., Kuchinski, L. E., Ramirez, S. V., Sellgren, K., Terndrup, D. M., & Tiede, G. P. 2000, AJ, 119, 536
Ford, W. K. Jr., Rubin, V. C., & Roberts, M. S. 1971, AJ, 76, 22
Funes, J. G., Corsini, E. M., Cappellari, M., Pizzella, A., Vega Beltrán, J. C., Scarlata, C., & Bertola, F. 2002, A&A, 388, 50
Irwin, J. A., Saika, D. J., & English, J. 2000, AJ, 119, 1592
Jarvis, B. J. 1986, AJ, 91, 65
Knapen, J. H., Shlosman, I., & Peletier, R. F. 2000, ApJ, 529, 93
Kuijken, K., & Merrifield, M. R. 1995, ApJ, 443, L13
Laurikainen, E., Salo, H., & Buta, R. 2004, ApJ, 607, 103
Lindblad, B. 1956, Stockholms Observatorium Annaler, Band 19, No. 2
Lütticke, R., Dettmar, R.-J., & Pohlen M. 2000a, A&AS, 145, 405
Lütticke, R., Dettmar, R.-J., & Pohlen M. 2000b, A&AS, 362, 435
Marinova, I., & Jogee, S. 2007, ApJ, 659, 1176
Martinez-Valpuesta, I., Knapen, J. H., & Buta, R. 2007, AJ, 134, 1863
Merrifield, M. & Kuijken, K. 1999 A&A, 345L, 47
Osterbrock, D. E., Fulbright, J. P., Martel, A. R., Keane, M. J., Trager, S. C., & Basri, G. 1996, PASP, 108, 277
Peterson, C. J., Rubin, V. C., Ford, W. K., Jr., & Thonnard, N. 1978, ApJ, 219, 31
Philips, M. M., Charles, P. A., & Baldwin, J. A. 1983, ApJ, 266, 485
Pompei, E., & Terndrup, D. M. 1999, in ASP Conf. Ser. 182, Galaxy Dynamics, ed. D. R. Merritt, M. Valluri, & J. A. Sellwood (San Francisco: ASP), 221
Raha, N., Sellwood, J. A., James, R. A., Kahn, F. D. 1991, Nature, 352, 411
Rowley, G. 1988, ApJ, 331, 124
Rubin, V. C. 1993, in Proc. Natl. Acad. Sci., 90, 4814
Schombert, J. 2007, arXiv:astro-ph/0703646
Shaw, M. A. 1987, MNRAS, 229, 691
Shaw, M. A. 1993, MNRAS, 261, 718
Sheth, K., Regan, M. W., Vogel, S. N., & Teuben, P. J. 2000, ApJ, 532, 221
Skrutskie, M. F., et al. 2006, AJ, 131, 1163
Stark, A. A., & Binney, J. 1994, ApJ, 426, L31
Teuben, P. J. The Stellar Dynamics Toolbox NEMO, in: Astronomical Data Analysis Software and Systems IV, ed. R. Shaw, H. E. Payne and J. J. E. Hayes. (1995), PASP Conf Series 77, p398
van den Bergh, S. 2002, AJ, 124, 782

Vega Beltrán, J. C., Pizzella, A., Corsini, E. M., Funes, J. G., Zeilinger, W. W., Beckman, J. E., & Bertola, F. 2001, A&A, 374, 394

Veilleux, S., & Osterbrock, D. E. 1987, ApJS, 63, 295

Verley, S., Combes, F., Verdes-Montenegro, L., Bergond, G., & Leon, S. 2007, A&A, 474, 43

Whyte, L. F., Abraham, R. G., Merrifield, M. R., Eskridge, P. B., Frogel, J. A., & Pogge, R. W. 2002, MNRAS, 336, 1281

Zurita, A., Relaño, M., Beckman, J. E., & Knapen, J. H. 2004, A&A, 413, 73